Engineering Transactions, **67**(3): 387–410, 2019, doi: 10.24423/EngTrans.954.20190725
Polish Academy of Sciences • Institute of Fundamental Technological Research (IPPT PAN)
Université de Lorraine • Poznan University of Technology

Research Paper

Impact of Thermophoretic Transport of Al_2O_3 Nanoparticles on Viscoelastic Flow of Oil-Based Nanofluid over a Porous Exponentially Stretching Surface with Activation Energy

Christian John ETWIRE[1)], Ibrahim Yakubu SEINI[2)*], Rabiu MUSAH[3)]
Oluwole Daniel MAKINDE[4)]

[1)] *Faculty of Mathematical Sciences*
University for Development Studies
P.O. Box 24, Navrongo, UER, Ghana

[2)] *School of Engineering*
University for Development Studies
Nyankpala Campus, P.O. Box 1882, Tamale, Ghana
[*]Corresponding Author e-mail: yakubuseini@yahoo.com

[3)] *Faculty of Applied Sciences*
University for Development Studies
P.O. Box 24, Navrongo, UER, Ghana

[4)] *Faculty of Military Science*
Stellenbosch University
Private Bag X2, Saldanha 7395, South Africa

The influence of thermophoretic transport of Al_2O_3 nanoparticles on heat and mass transfer in viscoelastic flow of oil-based nanofluid past porous exponentially stretching surface with activation energy has been examined. Similarity technique was employed to transform the governing partial differential equations into a coupled fourth-order ordinary differential equations which were reduced to a system of first-order ordinary differential equations and then solved numerically using the fourth-order Runge-Kutta algorithm with a shooting method. The results for various controlling parameters were tabulated and graphically illustrated. It was found that the thermophoretic transport of Al_2O_3 nanoparticles did not affect the rate of flow and heat transfer at the surface but it affected the rate of mass transfer of the nanofluid which decayed the solutal boundary layer thickness. This study also revealed that activation energy retards the rate of mass transfer which causes a thickening of the solutal boundary layer.

Key words: thermophoresis; activation energy; exponential stretching; deposition; nanofluid; thermophoretic.

Notations

(x, y) – Cartesian coordinates,
(u, v) – velocity components,
T_f – temperature of hot fluid,
T_∞ – free-stream temperature,
T_w – temperature of the sheet,
T – temperature of Al_2O_3 oil-based nanofluid,
k_f – thermal conductivity of oil,
k_s – thermal conductivity of Al_2O_3,
C – concentration of Al_2O_3 oil-based nanofluid,
C_∞ – free stream concentration of Al_2O_3 oil-based nanofluid,
D_B – Brownian diffusion coefficient,
c_p – specific heat at constant pressure,
k' – permeability of the porous media,
K^* – permeability parameter,
k_0 – coefficient of viscoelasticity,
Le – Lewis number,
h_f – heat transfer coefficient,
Pr – Prandtl number,
C_f – skin-friction coefficient,
Re – Reynolds number,
Nu – Nusselt number,
Sh – Sherwood number,
q_w – wall heat flux,
q_m – wall mass flux,
$\dot{q}$ – volumetric heat generation,
Bi – Biot number,
E – activation energy parameter,
Ec – Eckert number,
U_∞ – free stream velocity of Al_2O_3 oil-based nanofluid,
n – fitted rate constant,
V_T – thermophoretic deposition velocity,
S – suction parameter.

Greek Symbols

τ_w – wall shear stress,
μ_{nf} – dynamic viscosity of Al_2O_3 oil-based nanofluid,
υ_f – kinematic viscosity of oil,
ρ_{nf} – density of Al_2O_3 oil-based nanofluid,
α_f – thermal diffusivity of oil,
ρ_f – density of oil,
ρ_s – density of Al_2O_3,
φ – solid volume fraction of Al_2O_3,
$(\rho_{cp})_{nf}$ – heat capacitance of Al_2O_3 oil-based nanofluid,

ψ – stream function,
α – variable viscoelastic parameter of Al_2O_3 oil-based nanofluid,
λ – internal heat generation parameter,
β – chemical reaction rate parameter,
σ – thermal conductivity parameter of Al_2O_3 oil-based nanofluid,
Γ – thermophoresis parameter,
ω – temperature difference parameter.

1. Introduction

Thermophoretic deposition of particles in lubricants is a major concern to automobile engineers. The accumulation of these particles depletes the lifetime performance of lubricants and increases their viscosity index leading to high fuel consumption. Thermophoresis is a phenomenon observed in mixtures of mobile particles where the different particle types exhibit different responses to the force of a temperature gradient known as thermophoretic force. This force is used in precipitators, manufacture of optical fiber in vacuum deposition processes and transport mechanism in fouling [1]. In addition, tt is useful in accelerating drug delivery, manipulating single biological macro-molecules and separating different polymer particles in field flow fractionation [2].

Transport of thermophoretic particles occurs in many industrial and engineering processes such as exhaust gas recirculation coolers, electrical conduction, combustion chambers, and solar cells [3]. It is also common in tribological coating, thermoelectric devices, energy conservation and generation, semi-conductor devices, ion plating, sputter deposition, metallized film, molecular vapor deposition, magnetic films, diffusion barrier and lamp reflectors [4]. As a result, current research is directed at studying the effects of thermophoretic particle deposition phenomena and its impact on the heat and mass transfer characteristics of flow.

Thermophoresis and chemical reaction effects on magnetohydrodynamic (MHD) Darcy-Forchheimer mixed convection in a fluid saturated porous media with thermal-diffusion and diffusion-thermo effects were studied and reported in [5]. The effects of Brownian motion and thermophoresis on MHD mixed convection stagnation-point flow of a nanofluid toward a stretching vertical sheet in porous media with variable viscosity reacting flow were presented in [6]. The thermophoretic effect on a rotating cone in a porous medium with thermal radiation was reported in [7]. The effect of Brownian motion and thermophoresis on a nonlinear stretching permeable sheet in a nanofluid was reported by Falana *et al.* [8]. Raju *et al.* [9] investigated the thermophoresis effect on a radiating inclined permeable moving plate in the presence of chemical reaction and heat absorption.

Activation energy is a requirement in the initiation of a chemical reaction. It is the minimum amount of energy a reactive species must possess in order to undergo a specific reaction and is a very useful concept in chemical, geothermal and petrochemical engineering processes. The problem of heat and mass transfer mechanisms with activation energy has attracted the considerable interest of researchers. The boundary layer flow of Maxwell fluid in rotating frame with binary chemical reaction and activation energy was studied in [10], the effects of exothermic chemical reaction with Arrhenius activation energy in [11] and the non-uniform heat source or sink on MHD stagnation point flow of a Casson fluid over a nonlinear stretching sheet with variable fluid properties and slip conditions in [12]. The MHD mixed convection stagnation point flow with binary chemical reaction and activation energy over an inclined stretching sheet and Carreau fluid was presented in [13].

In the automobile industry, the depositions of particles into lubricants occur as a result of soot seeping into the engine oil sump through the piston rings. The high concentration of particulate in the engine oil erodes lubricated surfaces, imparting on the heat transfer within the lubrication boundary due to increase viscosity and friction effects. This causes severe engine wear which could lead to low engine performance. With the discovery of nanotechnology [14], the thermophysical properties of fluids are improved by introducing nano-sized particles into the fluid [15]. Similarly, the effect of Brownian motion and thermophoresis on nanofluids stretching in Jaffrey fluid model was discussed in [16] while the activation energy in Couette-Poiseuille flow of a nanofluid in the presence of chemical reaction and convective boundary conditions was reported in [17]. Variable thermophysical properties of thermophoretic viscoelastic fluid flow past a vertical surface were reported in [18].

From the available literature, the influence of thermophoretic particle deposition on heat and mass transfer characteristics of oil-based nanofluid is limited. The convectional thermophoresis particle depositions in oil lead to low thermal conductivity, particle sedimentation and excessive pressure drop.

This study examines the impact of thermophoretic transport of Al_2O_3 nanoparticles on heat and mass transfer in a viscoelastic flow of oil-based nanofluid over an exponentially stretching porous surface with activation energy.

2. Mathematical model

Consider a two-dimensional steady incompressible flow of dielectric and chemically reacting viscoelastic Al_2O_3 oil-based nanofluid over a permeable exponentially stretching plate with heat and mass transfer by convection in the presence of thermophoretic transport and activation energy. The x-axis is taken along the direction of the porous exponentially stretching plate while the y-axis is taken normal to it (Fig. 1). A stream of cold Al_2O_3 oil-based nanofluid at the free stream temperature T_∞ moves over the upper surface of the plate with a uniform free stream velocity U_∞ and free stream concentration C_∞ while the lower surface of the plate is heated by convection from a hot fluid at temperature T_f $\left(T_W = T_\infty + T_0 e^{x/2L}\right)$, which provides a heat transfer coefficient h_f with concentration $C_W = C_\infty + C_0 e^{x/2L}$. The Al_2O_3 oil-based nanofluid in contact with the lower surface of the plate generates heat internally at a volumetric rate $\dot{q}$. The velocity of the exponentially stretching plate is $u_w(x) = U_0 e^{x/L}$ directed along the x-axis.

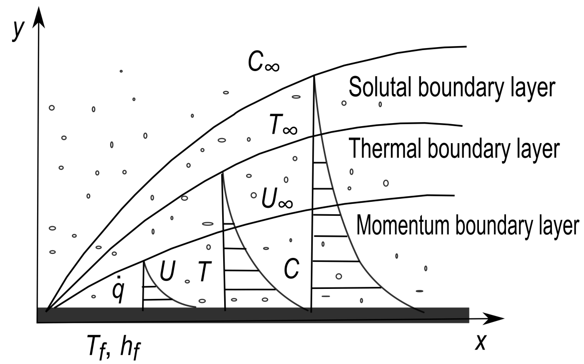

FIG. 1. Schematic diagram of the flow problem.

It is assumed that both the oil and Al_2O_3 nanoparticles are in thermal equilibrium with no slip between them. The variation of density in the Al_2O_3 oil-based nanofluid is taken into account using the Boussinesq approximation. The continuity, momentum and energy equations modeling the flow problem are

$$\frac{\partial u}{\partial x} + \frac{\partial v}{\partial y} = 0, \tag{2.1}$$

$$u\frac{\partial u}{\partial x} + v\frac{\partial u}{\partial y} = \frac{\mu_{nf}}{\rho_{nf}}\frac{\partial^2 u}{\partial y^2} - \frac{\mu_{nf}}{\rho_{nf}k'}u - \frac{k_0}{\rho_{nf}}\left(v\frac{\partial^3 u}{\partial y^3} + u\frac{\partial^3 u}{\partial x \partial y^2} + \frac{\partial u}{\partial x}\frac{\partial^2 u}{\partial y^2} - \frac{\partial u}{\partial y}\frac{\partial^2 u}{\partial x \partial y}\right), \tag{2.2}$$

$$u\frac{\partial T}{\partial x} + v\frac{\partial T}{\partial y} = \frac{1}{(\rho c_p)_{nf}}\frac{\partial}{\partial y}\left(k_{nf}(T)\frac{\partial T}{\partial y}\right) + \frac{\mu_{nf}}{(\rho c_p)_{nf}}\left(\frac{\partial u}{\partial y}\right)^2 + \frac{k_0}{(\rho c_p)_{nf}}\left(u\frac{\partial^2 u}{\partial x \partial y}\frac{\partial u}{\partial y} + v\frac{\partial^2 u}{\partial y^2}\frac{\partial u}{\partial y}\right) + \dot{q}, \tag{2.3}$$

$$u\frac{\partial C}{\partial x}+v\frac{\partial C}{\partial y}=D_B\frac{\partial^2 C}{\partial y^2}-K_r^2\left(C-C_\infty\right)\left(\frac{T}{T_\infty}\right)^n e^{\left(-\frac{Ea}{K^*T}\right)} -\frac{\partial}{\partial y}\left(V_T(C-C_\infty)\right), \tag{2.4}$$

where u and v are x and y components of velocities respectively, μ_{nf} is the dynamic viscosity of Al_2O_3 oil-based nanofluid, $k_{nf}(T)$ is the temperature-dependent thermal conductivity of Al_2O_3 oil-based nanofluid, ρ_{nf} is the density of Al_2O_3 oil-based nanofluid, k' is the permeability of the porous media, k_0 is the coefficient of viscoelasticity, T is the temperature of Al_2O_3 oil-based nanofluid, $(\rho c_p)_{nf}$ is the heat capacitance of Al_2O_3 oil-based nanofluid, C is the concentration of Al_2O_3 oil-based nanofluid, D_B is the Brownian diffusion coefficient, and V_T is the thermophoretic deposition velocity. The term $K_r^2\left(C-C_\infty\right)\left(\frac{T}{T_\infty}\right)^n e^{\left(-\frac{Ea}{K^*T}\right)}$ in Eq. (2.4) denotes Arrhenius expression where K_r^2 is the chemical reaction rate constant, E_a is the activation energy, $K^*=8.61\cdot 10^{-5}$ eV/K is the permeability parameter, and n is the fitted rate constant which lies in the range $-1<n<1$.

The boundary conditions on the surface of the plate are

$$\begin{gathered} u(x,0)=U_0e^{x/L},\quad v(x,0)=-v_w,\quad -k_f\frac{\partial T}{\partial y}(x,0)=h_f[T_w-T(x,0)],\\ C=C_w\quad\text{at}\quad y=0. \end{gathered}\tag{2.5}$$

The boundary conditions far away from the surface of the plate are

$$\begin{gathered} u(x,\infty)\to 0,\qquad \frac{\partial u(x,\infty)}{\partial y}\to 0,\qquad T(x,\infty)\to T_\infty,\\ C\to C_\infty,\quad\text{as}\quad y\to\infty. \end{gathered}\tag{2.6}$$

The temperature-dependent thermal conductivity $k_{nf}(T)$ and the thermal thermophoretic deposition V_T are defined respectively as

$$k_{nf}(T)=k_{nf}\left(1+Q\frac{T-T_\infty}{T_w-T_\infty}\right)\qquad\text{and}\qquad V_T=-\gamma\frac{v_f}{T_r}\frac{\partial T}{\partial y},\tag{2.7}$$

where k_{nf} is the thermal conductivity oil-based nanofluid, γ is the thermophoresis coefficient, and v_f is the kinematic viscosity of the oil. The properties of the nanofluid with spherical sized Al_2O_3 nanoparticles are defined in [19] as

$$\begin{gathered} \mu_{nf}=\frac{\mu_f}{(1-\varphi)^{2.5}},\qquad \frac{k_{nf}}{k_f}=\frac{(k_s+2k_f)-2\varphi\left(k_f-k_s\right)}{(k_s+2k_f)+\varphi\left(k_f-k_s\right)},\\ \left(\rho c_p\right)_{nf}=(1-\varphi)\left(\rho c_p\right)_f+\varphi\left(\rho c_p\right)_s,\qquad \rho_{nf}=(1-\varphi)\,\rho_f+\varphi\rho_s, \end{gathered}\tag{2.8}$$

where ρ_f and ρ_s are the densities of the oil and solid volume fraction of Al_2O_3 respectively, φ is the solid volume fraction of Al_2O_3, k_f and k_s are the thermal conductivities of the oil and Al_2O_3 nanoparticles respectively, and $\mu_f = \upsilon_f \rho_f$ is the dynamic viscosity of the oil.

3. Similarity transformations

The stream function $\psi(x, y)$ is defined in the usual way as

$$u = \frac{\partial \psi}{\partial y} \quad \text{and} \quad v = -\frac{\partial \psi}{\partial x}. \tag{3.1}$$

Equation (3.1) satisfies the continuity Eq. (2.1) automatically.

A similarity solution of Eqs (2.1)–(2.5) is achieved by defining an independent dimensionless variable η, a stream function ψ, in terms of a dependent variable $f(\eta)$, a dimensionless temperature $\theta(\eta)$ and a dimensionless concentration $\phi(\eta)$ as

$$\begin{aligned} \eta &= y\sqrt{\frac{U_0}{2L\upsilon_f}}e^{x/2L}, \qquad & \psi &= \sqrt{2L\upsilon_f U_0} f(\eta) e^{x/2L}, \\ \theta(\eta) &= \frac{T - T_\infty}{T_0 e^{x/2L}}, \qquad & \phi(\eta) &= \frac{C - C_\infty}{C_0 e^{x/2L}}. \end{aligned} \tag{3.2}$$

Substituting relevant terms into Eqs (2.1)–(2.5) yields the coupled ordinary differential equations as

$$\begin{aligned} &\frac{\rho_f}{(1-\varphi)^{2.5}\left[(1-\varphi)\rho_f + \varphi\rho_s\right]} f''' + f f'' - 2f'^2 \\ &\qquad - \frac{2K^*\rho_f}{(1-\varphi)^{2.5}\left[(1-\varphi)\rho_f + \varphi\rho_s\right]} f' \\ &\qquad - \frac{\rho_f \alpha}{(1-\varphi)\rho_f + \varphi\rho_s}\left[3f'f''' - \frac{3}{2}f''^2 - \frac{1}{2}f f''''\right] = 0, \end{aligned} \tag{3.3}$$

$$\begin{aligned} &\frac{(k_s + 2k_f) - 2\varphi(k_f - k_s)}{(k_s + 2k_f) + \varphi(k_f - k_s)}\left[(1+\sigma\theta)\theta'' + \sigma\theta'^2\right] \\ &\qquad + \frac{(1-\varphi)(\rho c_p)_f + \varphi(\rho c_p)_s}{(\rho c_p)_f} \Pr\left(f\theta' - f'\theta\right) \\ &\qquad + \frac{\Pr \mathrm{Ec}}{(1-\varphi)^{2.5}} f''^2 + \Pr \mathrm{Ec}\, \alpha\left(\frac{3}{2}f'f''^2 - \frac{1}{2}f f'' f'''\right) + 2\lambda e^{-\eta} = 0, \end{aligned} \tag{3.4}$$

$$\phi'' - \Pr \mathrm{Le} f'\phi + \Pr \mathrm{Le} f\phi' - 2\Pr \mathrm{Le}\beta(1+\omega\theta)^n e^{-\frac{\Lambda}{1+\omega\theta}}\phi + \Pr \mathrm{Le}\, \Gamma\left(\theta'\phi' + \phi\theta''\right) = 0 \tag{3.5}$$

subject to the boundary conditions:

$$\begin{aligned} &f'(0) = 1, \quad f(0) = S, \quad \theta'(0) = -\mathrm{Bi}(1-\theta(0)), \quad \phi(0) = 1, \quad \text{at} \quad \eta = 0, \\ &f'(\infty) \to 0, \quad f''(\infty) \to 0, \quad \theta(\infty) \to 0, \quad \phi(\infty) \to 0, \quad \text{as} \quad \eta \to \infty, \end{aligned} \tag{3.6}$$

where the prime symbol denotes differentiation with respect to η, $K^* = \frac{\upsilon_f L}{k' U_0 e^{x/L}}$ is the permeability parameter, $\alpha = \frac{k_0 U_0 e^{x/L}}{L\mu_f}$ is the local viscoelastic parameter, $S = \frac{V_w}{\sqrt{\frac{U_0}{2L\upsilon_f}e^{x/2L}}}$ is the local suction parameter, $\Pr = \frac{\upsilon_f}{\alpha_f}$ is the Prandtl number, $\mathrm{Bi} = \frac{h_f}{k_f\sqrt{\frac{U_0}{2L\upsilon_f}e^{x/2L}}}$ is the local Biot number, $\lambda = \frac{L\dot{q}\upsilon_f e^{\eta}}{k_f T_0 U_0 e^{3x/2L}}$ is the local internal heat generation parameter, $\beta = \frac{LK_r^2}{U_0 e^{x/L}}$ is the local chemical reaction rate parameter, $\mathrm{Le} = \frac{\alpha_f}{D_B}$ is the Lewis number, $\sigma = Q\frac{T_0 e^{x/2L}}{T_w - T_\infty}$ is the local thermal conductivity parameter, $\Gamma = \frac{T_0 e^{x/L}\gamma}{T_r}$ is the local thermophoresis parameter, $\omega = \frac{T_0 e^{x/2L}}{T_\infty}$ is the local temperature difference parameter, $E = \frac{Ea}{k_f T_\infty}$ is the activation energy parameter, and $\mathrm{Ec} = \frac{U_0^2 e^{3x/2L}}{k_f (C_p)_f}$ is the local Eckert number.

The parameters of engineering importance are the skin-friction coefficient (C_f), the Nusselt number (Nu) and the Sherwood number (Sh) which are defined respectively as

$$C_f = \frac{\tau_w}{\rho_f u_w^2}, \quad \mathrm{Nu} = \frac{x q_w}{k_f (T_w - T_\infty)}, \quad \text{and} \quad \mathrm{Sh} = \frac{x q_m}{D_B (C_w - C_\infty)}, \tag{3.7}$$

where τ_w is the wall shear stress, q_w is the wall heat flux, and q_m is the wall mass flux which are given respectively by:

$$\begin{aligned} \tau_w &= \left[\mu_{nf}\frac{\partial u}{\partial y} + \frac{k_0}{\rho_{nf}}\left(u\frac{\partial^2 u}{\partial x \partial y} + v\frac{\partial^2 u}{\partial y^2} - 2\frac{\partial u}{\partial y}\frac{\partial v}{\partial y}\right)\right]_{y=0}, \\ q_w &= -k_{nf}\left.\frac{\partial T}{\partial y}\right|_{y=o}, \\ q_m &= -D_B\left.\frac{\partial C}{\partial y}\right|_{y=0}. \end{aligned} \tag{3.8}$$

Substituting Eq. (3.8) into Eq. (3.7) yields

(3.9)
$$C_f = \sqrt{\frac{1}{2\mathrm{Re}_x}}\left[\left(\frac{1}{(1-\varphi)^{2.5}} + \frac{7\alpha}{2\left((1-\varphi)\rho_f + \varphi\rho_s\right)}\right) f''(0) - \frac{\alpha S}{2\left((1-\varphi)\rho_f + \varphi\rho_s\right)} f'''(0)\right],$$

$$\mathrm{Nu} = -\frac{x}{L}\frac{(k_s + 2k_f) - 2\varphi(k_f - k_s)}{(k_s + 2k_f) + \varphi(k_f - k_s)}\sqrt{\frac{\mathrm{Re}_x}{2}}\,\theta'(0),$$

$$\mathrm{Sh} = -\frac{x}{L}\sqrt{\frac{\mathrm{Re}_x}{2}}\,\phi'(0),$$

where $\mathrm{Re}_x = \frac{U_w L}{\upsilon_f}$ is the local Reynolds number.

4. Numerical procedure

The coupled order nonlinear ordinary differential equations were reduced to a system of first-order ordinary differential equations by letting

(4.1)
$$\begin{aligned} f &= x_1, & f' &= x_2, & f'' &= x_3, & f''' &= x_4, \\ \theta &= x_5, & \theta' &= x_6, & \phi &= x_7, & \phi' &= x_8. \end{aligned}$$

Substituting into Eqs (3.3)–(3.6) yields the required first-order system of ordinary differential equations as

(4.2)
$$\begin{aligned} f' &= x_1' = x_2, \\ f'' &= x_2' = x_3, \\ f''' &= x_3' = x_4, \\ f'''' &= x_4' = \frac{2}{x_1}\left[3x_2x_4 - \frac{3}{2}x_3^2 - \frac{(1-\varphi)\rho_f + \varphi\rho_s}{\rho_f\alpha}\right. \\ &\quad \left.\cdot\left(x_4 + \frac{(1-\varphi)^{2.5}\left[(1-\varphi)\rho_f + \varphi\rho_s\right]}{\rho_f}\left(x_1x_3 - 2x_2^2\right) - 2K^*x_2\right)\right], \end{aligned}$$

$$\theta' = x_6,$$

$$\theta'' = x_6' = -\frac{1}{(1+\sigma x_5)}\left[\sigma x_6^2 + \frac{(k_s+2k_f)+\varphi(k_f-k_s)}{(k_s+2k_f)-2\varphi(k_f-k_s)}\right.$$

$$\cdot\left(\frac{(1-\varphi)(\rho c_p)_f+\varphi(\rho c_p)_s}{(\rho c_p)_f}\Pr(x_1x_6-x_2x_5)+\frac{\Pr\mathrm{Ec}}{(1-\varphi)^{2.5}}x_3^2\right.$$

$$\left.\left.+\Pr\mathrm{Ec}\,\alpha\left(\frac{3}{2}x_2x_3^2-\frac{1}{2}xx_3x_4\right)+2\lambda e^{-\eta}\right)\right],$$

(4.2)[Cont.] $$\phi' = x_8,$$

$$\phi'' = x_8' = \Pr\mathrm{Le}\,x_2x_7 - \Pr\mathrm{Le}\,x_1x_8 2\Pr\mathrm{Le}\,\beta(1+\omega x_5)^n e^{-\frac{E}{1+\omega x_5}}x_7$$

$$-\Pr\mathrm{Le}\,\Gamma\left(x_6x_8 - x_7\frac{1}{(1+\sigma x_5)}\left[\sigma x_6^2+\frac{(k_s+2k_f)+\varphi(k_f-k_s)}{(k_s+2k_f)-2\varphi(k_f-k_s)}\right.\right.$$

$$\cdot\left(\frac{(1-\varphi)(\rho c_p)_f+\varphi(\rho c_p)_s}{(\rho c_p)_f}\Pr(x_1x_6-x_2x_5)+\frac{\Pr\mathrm{Ec}}{(1-\varphi)^{2.5}}x_3^2\right.$$

$$\left.\left.\left.+\Pr\mathrm{Ec}\,\alpha\left(\frac{3}{2}x_2x_3^2-\frac{1}{2}xx_3x_4\right)+2\lambda e^{-\eta}\right)\right]\right)$$

subject to the boundary conditions

$$\begin{aligned} &x_2 = 1, \quad x_1 = s_1, \quad x_6 = -\mathrm{Bi}(1-d), \quad x_7 = 1,\\ &x_2 = s_2, \quad x_3 = s_3, \quad x_5 = s_4, \quad x_7 = s_5. \end{aligned} \tag{4.3}$$

The unknown boundary conditions s_1, s_2, s_3, s_4, s_5 were approximated using the Shooting technique and the resulting initial value problem solved using the fourth order Runge Kutta integration scheme. Numerical computations were done using MAPLE 16 software package.

5. Results and discussion

The embedded parameters controlling the flow dynamics are the thermal conductivity parameter (σ), internal heat generation parameter (λ), suction parameter (S), Biot number (Bi), fitted rate constant (n), Eckert number (Ec), Prandtl number (Pr), Lewis number (Le), permeability parameter (K^*), solid volume fraction of Al_2O_3 (φ), viscoelastic parameter (α), thermophoresis parameter (Γ), activation energy parameter (E), reaction rate parameter (β), and temperature difference parameter (ω).

The effects of these parameters on the velocity profile, temperature profile, skin friction coefficient (C_f), Nusselt number (Nu) and Sherwood number (Sh) were studied. The solid volume fraction of Al_2O_3 was varied within the range $0 \leq \phi \leq 0.1$. The thermophysical properties of oil and Al_2O_3 are presented in Table 1.

Table 1. Thermophysical properties of oil-based fluid and nanoparticle.

Physical property	C_p [J/(kg · K)]	ρ [kg/m^3]	k [W/mK]
Oil	1670	920	0.138
Al_2O_3	765	3970	40

5.1. Numerical results

Results of the present work for the Nusselt number denoted by $(-\theta'(0))$ were compared with the work of Bidin and Nazar [20] for varying Prandtl number (Pr) and Eckert number (Ec) when $\lambda = K = n = \omega = E = \sigma = \Gamma = \beta = S = \text{Bi} = \varphi = \text{Le} = \alpha = K^* = 0$ with the boundary condition $\theta(0) = 1$ for non-convective flow. The excellent agreement of the results up to three decimal of places validated the present work (see Table 2).

Table 2. Computations showing comparison with Bidin and Nazar [20] for $\lambda = K = n = \omega = E = \sigma = \Gamma = \text{Le} = \beta = S = \text{Bi} = \varphi = \alpha = K^* = 0$.

	Bidin and Nazar [20]		Present work	
	Ec – 0	Ec – 0.9	Ec – 0	Ec – 0.9
Pr	$-\theta'(0)$	$-\theta'(0)$	$-\theta'(0)$	$-\theta'(0)$
1	0.9547	0.5385	0.9548	0.5386
2	1.4714	0.7248	1.4715	0.7248
3	1.8691	0.8301	1.8691	0.8301

The impact of the various thermo-physical parameters on the skin friction coefficient ($f''(\theta)$), Nusselt number ($\theta'(0)$) and Sherwood number ($\phi(0)$) are presented in Table 3.

It is observed in Table 3 that the intensity of the thermophoresis parameter did not influence both the skin friction coefficient and Nusselt number but increased the magnitude of the Sherwood number. This is because a rise in the thermophoresis parameter leads to a higher mass transfer of Al_2O_3 nanoparticles in the oil due to convective mass transport. A similar trend was observed with

Table 3. Computation showings of $-f''(0)$, $-\theta'(0)$ and $-\phi'(0)$ for varying parameter values.

Γ	n	ω	Le	β	E	Bi	Pr	σ	Ec	λ	φ	α	K^*	S	$-f''(0)$	$-\theta'(0)$	$-\phi'(0)$
0.01	1	0.1	0.1	0.1	0.1	0.1	100	0.1	0.1	1	0.01	1	0.1	0.1	0.584502	0.072685	4.534894
0.02															0.584502	0.072685	4.557179
0.03															0.584502	0.072685	4.579559
	2														0.584502	0.072685	4.538667
	3														0.584502	0.072685	4.542562
	4														0.584502	0.072685	4.546581
		0.5													0.584502	0.072685	4.550886
		1.0													0.584502	0.072685	4.570771
		2.0													0.584502	0.072685	4.610182
			0.4												0.584502	0.072685	10.566823
			0.7												0.584502	0.072685	15.208225
			1.0												0.584502	0.072685	19.370494
				1											0.584502	0.072685	5.472635
				2											0.584502	0.072685	6.339914
				3											0.584502	0.072685	7.093421
					1										0.584502	0.072685	4.466656
					2										0.584502	0.072685	4.435842
					3										0.584502	0.072685	4.424079
						1.0									0.584502	0.692889	4.588860
						5.0									0.584502	2.863014	4.777570
						9.0									0.584502	4.382933	4.909630
							110								0.584502	0.074354	4.797737
							120								0.584502	0.075727	5.051673
							130								0.584502	0.076875	5.297829

Table 3. [Cont.]

Γ	n	ω	Le	β	E	Bi	Pr	σ	Ec	λ	φ	α	K^*	S	$-f''(0)$	$-\theta'(0)$	$-\phi'(0)$
								1							0.584502	0.072040	4.533537
								2							0.584502	0.071400	4.532286
								3							0.584502	0.070825	4.531232
									0.2						0.584502	0.061936	4.536067
									0.3						0.584502	0.051187	4.537230
									0.4						0.584502	0.040437	4.538384
										2					0.584502	0.056540	4.551115
										3					0.584502	0.040303	4.567287
										4					0.584502	0.023974	4.583410
											0.02				0.568010	0.073061	4.537427
											0.03				0.548383	0.073514	4.540624
											0.04				0.525659	0.074033	4.544466
												1.10			0.657689	0.070114	4.521059
												1.20			0.708917	0.067873	4.511415
												1.25			0.728090	0.066883	4.507863
													0.11		0.603587	0.071988	4.530397
													0.12		0.622438	0.071289	4.525939
													0.13		0.641060	0.070586	4.521520
														0.101	0.586858	0.072581	4.540653
														0.105	1.005739	0.057124	4.468222
														0.110	1.724238	0.023238	4.321520

changes in fitted rate constant, temperature difference parameter, Lewis number and chemical reaction rate parameter. However, the activation energy parameter depletes the Sherwood number as a result of the enhancement of the diffusive mass transport of Al_2O_3 nanoparticles.

Furthermore, it is noted that the combined impact of the Biot and Prandtl numbers enhanced both the Nusselt and Sherwood numbers due to convective heat and mass transfer of Al_2O_3 oil-based nanofluid at the surface of the plate. By contrast, the thermal conductivity parameter decreases both the Nusselt and the Sherwood numbers. An increase in the thermal conductivity parameter corresponds to a rise in the temperature of the Al_2O_3 oil-based nanofluid. Since temperature is inversely proportional to viscosity, the Al_2O_3 oil-based nanofluid becomes more viscous thereby retarding the rates of heat and mass transfer at the surface of the plate. Furthermore, a simultaneous rise in both the Eckert number and internal heat generation parameters deteriorates the Nusselt number but tends to enhance the Sherwood number due to the decaying of the heat and improvement in the rate of mass transfer near the surface of the plate.

Additionally, the high solid volume fraction of Al_2O_3 depreciates the skin friction coefficient but tends to enhance the magnitude of both the Nusselt and Sherwood numbers due to the ballistic collision of the nanoparticles. Increasing the viscoelastic, permeability and suction parameters leads to the decreased skin friction coefficient, Nusselt number and Sherwood number.

5.2. Graphical results

5.2.1. Velocity profiles. The influence of various thermophysical parameters on the velocity profiles is illustrated in Figs 2–5. The effect of the viscoelastic

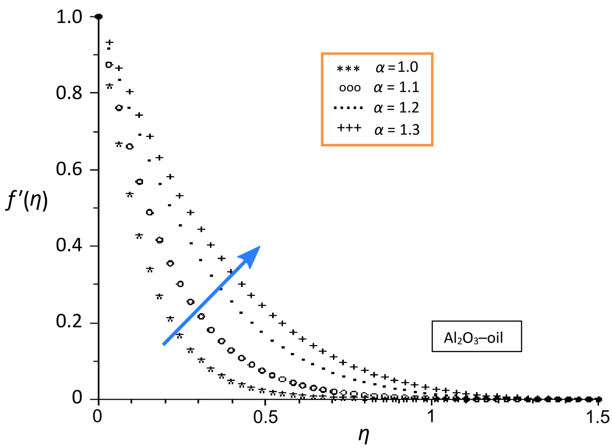

FIG. 2. Velocity profile for varying values of viscoelastic parameter for $\Pr = 100$, $S = 0.1$, $\mathrm{Bi} = 0.1$, $K^* = 0.1$, $\lambda = 1$, $\mathrm{Le} = 0.1$, $\sigma = 0.1$, $E = 0.1$, $\beta = 0.1$, $n = 1$, $\omega = 0.1$, $\varGamma = 0.1$, $\mathrm{Ec} = 0.1$, and $\varphi = 0.01$.

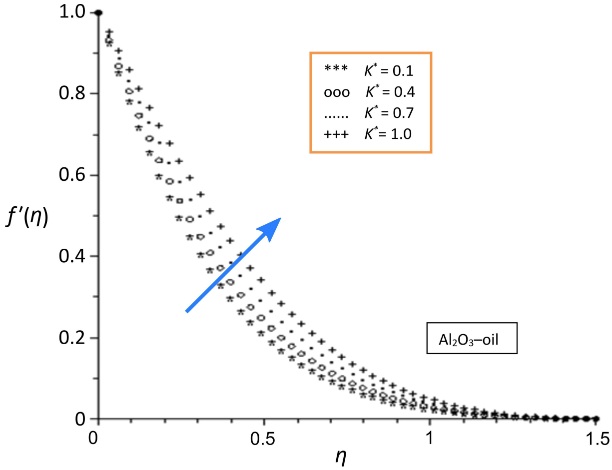

FIG. 3. Velocity profile for varying values of permeability parameter for $\mathrm{Pr} = 100$, $\alpha = 1$, $S = 0.2$, $\mathrm{Bi} = 0.1$, $\lambda = 1$, $\mathrm{Le} = 0.1$, $\sigma = 0.1$, $E = 0.1$, $\beta = 0.1$, $n = 1$, $\omega = 0.1$, $\Gamma = 0.1$, $\mathrm{Ec} = 0.1$, and $\varphi = 0.01$.

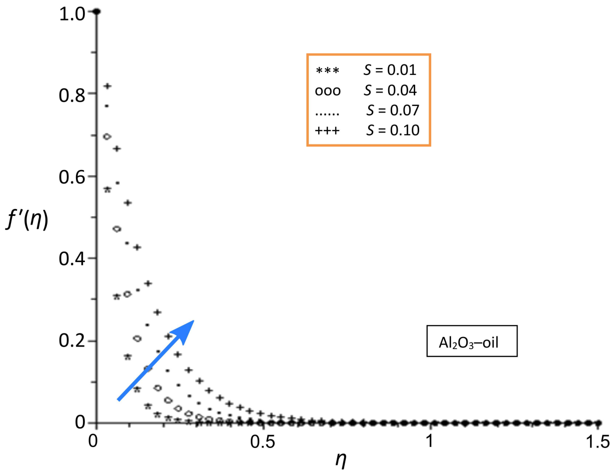

FIG. 4. Velocity profile for varying values of suction parameter for $\mathrm{Pr} = 100$, $\alpha = 1$, $K^* = 0.1$, $\mathrm{Bi} = 0.1$, $\lambda = 1$, $\mathrm{Le} = 0.1$, $\sigma = 0.1$, $E = 0.1$, $\beta = 0.1$, $n = 1$, $\omega = 0.1$, $\Gamma = 0.1$, $\mathrm{Ec} = 0.01$, and $\varphi = 0.01$.

parameter on the velocity of the Al_2O_3 oil-based nanofluid within the boundary layer is depicted in Fig. 2. It is observed that the viscoelastic parameter increases the flow of the oil-based nanofluid as a result of the reduction in its viscosity. Higher values of the viscoelastic parameter make the Al_2O_3 oil-based nanofluid more elastic and viscous, but the internal heating of the nanofluid decreases its viscosity resulting in an increased velocity within the boundary layer which makes the momentum boundary layer thicker.

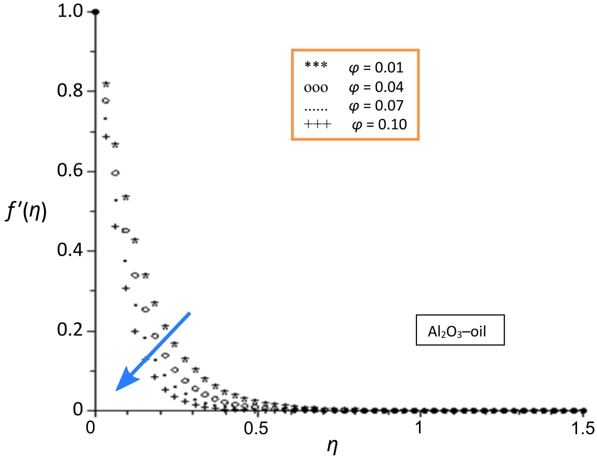

FIG. 5. Velocity profile for varying values of solid volume fraction of Al_2O_3 nanoparticles for $\mathrm{Pr} = 100$, $\alpha = 1$, $K^* = 0.1$, $\mathrm{Bi} = 0.1$, $\lambda = 1$, $\mathrm{Le} = 0.1$, $\sigma = 0.1$, $E = 0.1$, $\beta = 0.1$, $n = 1$, $\omega = 0.1$.

Figures 3 and 4 illustrate the velocity profiles for increasing values of the permeability and suction parameters respectively. The velocity profiles of these figures follow a similar trend as that of Fig. 2 due to viscous dissipation. However, Fig. 5 shows that higher values of the solid volume fraction of Al_2O_3 nanoparticles retard the velocity of the Al_2O_3 oil-based nanofluid within the boundary layer as a result of the clustering of the Al_2O_3 nanoparticles. This causes a deterioration of the momentum boundary layer thickness.

5.2.2. Temperature profiles. The effects of thermophysical parameters on the temperature profiles are presented in Figs 6–14. The impact of the solid vol-

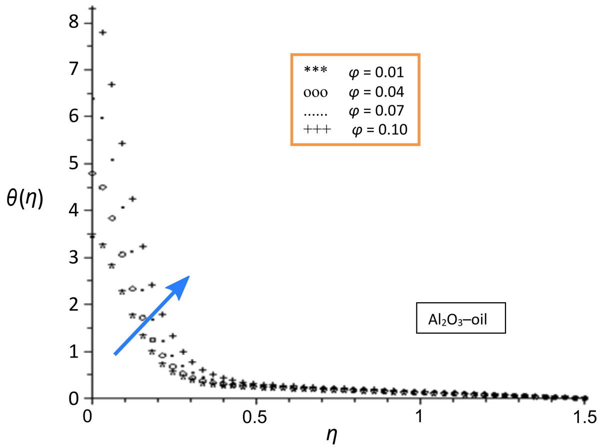

FIG. 6. Temperature profile for varying values of solid volume fraction of Al_2O_3 nanoparticles for $\mathrm{Pr} = 100$, $\alpha = 1$, $K^* = 0.1$, $\mathrm{Bi} = 0.1$, $\lambda = 1$, $\mathrm{Le} = 0.1$, $\sigma = 0.1$, $E = 0.1$, $\beta = 0.1$, $n = 1$, $\omega = 0.1$, $\Gamma = 0.1$, $\mathrm{Ec} = 0.1$, and $S = 0.1$.

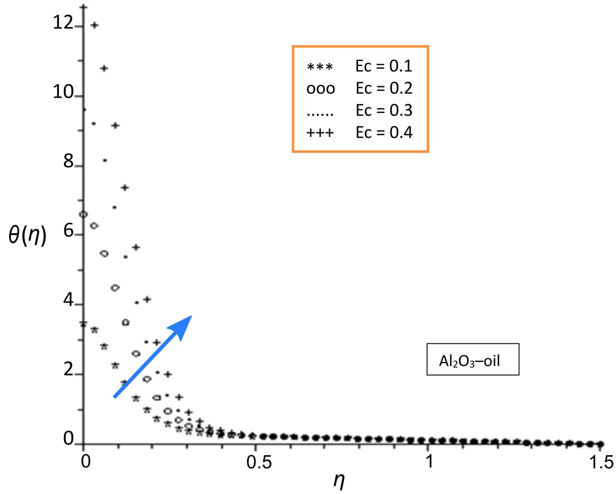

FIG. 7. Temperature profile for varying values of Eckert number for $\mathrm{Pr} = 100$, $\alpha = 1$, $K^* = 0.1$, $\mathrm{Bi} = 0.1$, $\lambda = 1$, $\mathrm{Le} = 0.1$, $\sigma = 0.1$, $E = 0.1$, $\beta = 0.1$, $n = 1$, $\omega = 0.1$, $\Gamma = 0.1$, $\varphi = 0.01$, and $S = 0.1$.

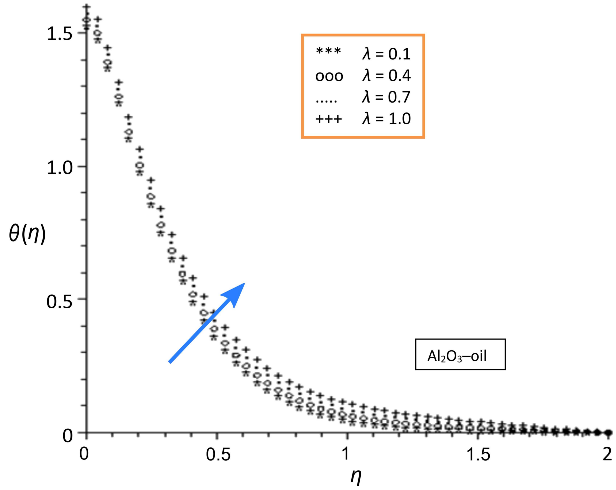

FIG. 8. Temperature profile for varying values of internal heat generation parameter for $\mathrm{Pr} = 100$, $\alpha = 1$, $K^* = 0.1$, $\mathrm{Ec} = 0.5$, $\mathrm{Bi} = 0.1$, $\mathrm{Le} = 0.1$, $\sigma = 0.1$, $E = 0.1$, $\beta = 0.1$, $n = 1$, $\omega = 0.1$, $\Gamma = 0.1$, $\varphi = 0.01$, and $S = 0.2$.

ume fraction of Al_2O_3 nanoparticles on the temperature is depicted in Fig. 6. The solid volume fraction increases the temperature within the boundary layer leading to a thicker thermal boundary layer. A similar trend is observed in Figs 7–9 with increasing the values of the Eckert number, internal heat generation parameter and thermal conductivity.

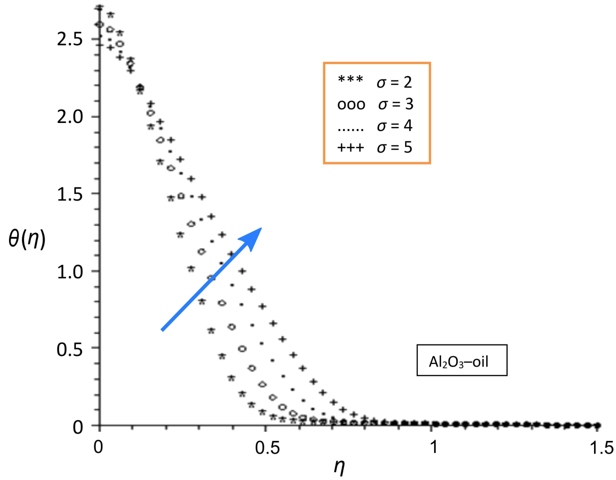

FIG. 9. Temperature profile for varying values of thermal conductivity parameter for $\mathrm{Pr} = 100$, $\alpha = 1$, $K^* = 0.1$, $\mathrm{Ec} = 0.1$, $\mathrm{Bi} = 0.1$, $\mathrm{Le} = 0.1$, $\lambda = 0.1$, $E = 0.1$, $\beta = 0.1$, $n = 1$, $\omega = 0.1$, $\Gamma = 0.1$, $\varphi = 0.01$, and $S = 0.1$.

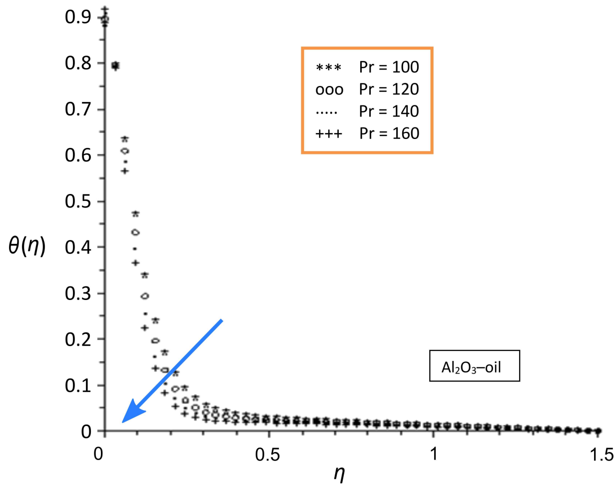

FIG. 10. Temperature Profile for varying values of Prandtl number for $\alpha = 1$, $S = 0.1$, $K^* = 0.1$, $\mathrm{Bi} = 1$, $\lambda = 0.1$, $\mathrm{Le} = 0.1$, $\sigma = 0.1$, $E = 0.1$, $\beta = 0.1$, $n = 1$, $\omega = 0.1$, $\Gamma = 0.1$, $\mathrm{Ec} = 0.01$, and $\varphi = 0.1$.

In practice, an increase in the viscoelastic parameter corresponds to a rise in temperature, but the temperature within the boundary layer region decreases due to the retarding rate of heat transfer. This is as a result of the sucking away of the nanofluid through the porous media. Figures 9–11 illustrate the influence cof the Prandtl number and suction parameter on the thermal boundary layer thickness. Higher values of these parameters make the thermal boundary layer thinner due to the deterioration of the thermal diffusivity.

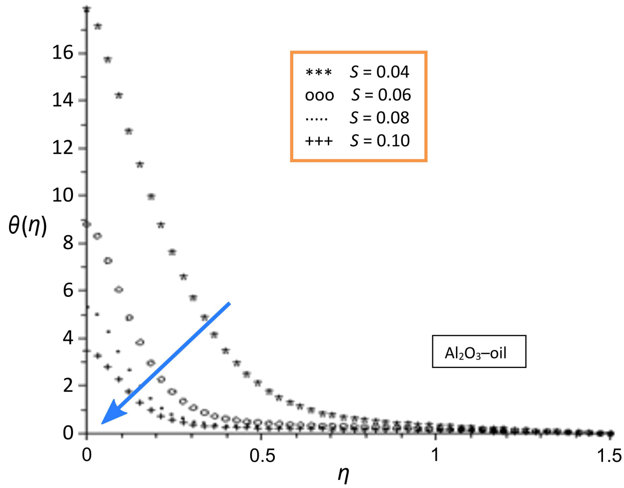

FIG. 11. Temperature profile for varying values of suction parameter for $\mathrm{Pr} = 100$, $\alpha = 1$, $K^* = 0.1$, $\mathrm{Bi} = 0.1$, $\lambda = 1$, $\mathrm{Le} = 0.1$, $\sigma = 0.1$, $E = 0.1$, $\beta = 0.1$, $n = 1$, $\omega = 0.1$, $\Gamma = 0.1$, $\mathrm{Ec} = 0.01$, and $\varphi = 0.01$.

5.2.3. The concentration profiles. Figures 12–18 depict the influence of various thermophysical parameters on the concentration boundary layer. Figures 12 and 13 show that thermal conductivity and the viscoelastic parameter enhance the solutal boundary layer thickness. This means that an increase in thermal conductivity of the nanofluid enhances particle mobility resulting in an increased chemical reaction within the boundary layer.

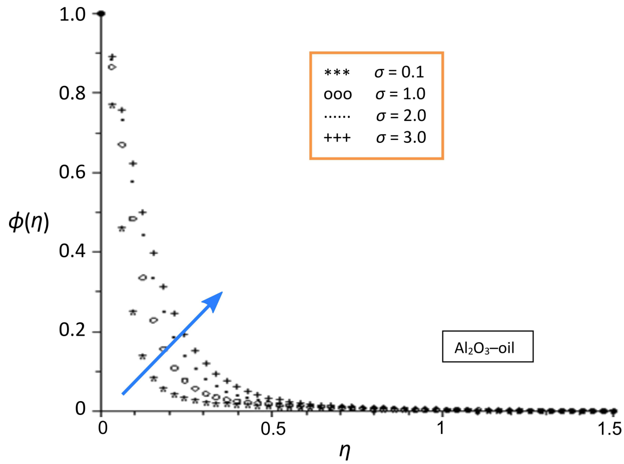

FIG. 12. Concentration profile for varying values of thermal conductivity parameter for $\mathrm{Pr} = 100$, $\alpha = 1$, $K^* = 0.1$, $\mathrm{Ec} = 0.1$, $\mathrm{Bi} = 0.1$, $\mathrm{Le} = 0.1$, $\lambda = 1$, $E = 0.1$, $\beta = 0.1$, $n = 1$, $\omega = 0.1$, $\Gamma = 0.1$, $\varphi = 0.01$, and $S = 0.1$.

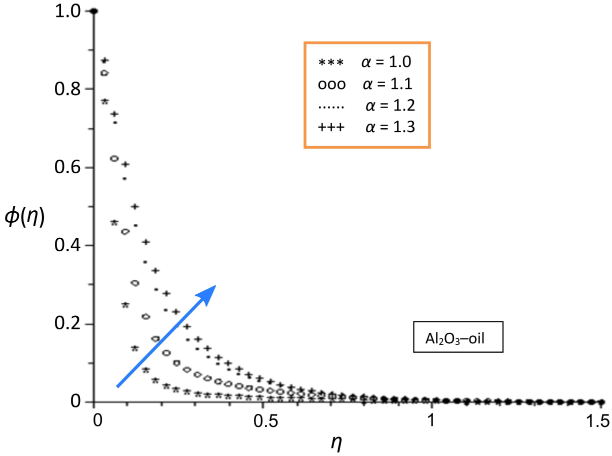

FIG. 13. Concentration profile for varying values of viscoelastic parameter for $\mathrm{Pr} = 100$, $S = 0.1$, $K^* = 0.1$, $\mathrm{Bi} = 0.1$, $\lambda = 1$, $\mathrm{Le} = 0.1$, $\sigma = 0.1$, $E = 0.1$, $\beta = 0.1$, $n = 1$, $\omega = 0.1$, $\Gamma = 0.1$, $\mathrm{Ec} = 0.1$, and $\varphi = 0.01$.

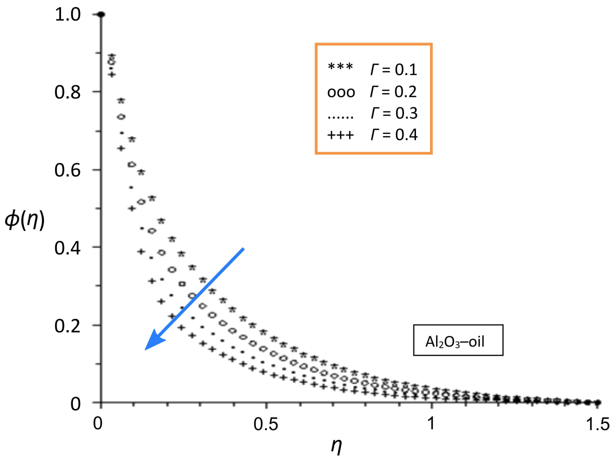

FIG. 14. Concentration profile for varying values of thermophoresis parameter for $\mathrm{Pr} = 100$, $\alpha = 1$, $K^* = 0.1$, $\mathrm{Ec} = 0.1$, $\mathrm{Bi} = 0.1$, $\mathrm{Le} = 0.1$, $\lambda = 1$, $E = 0.1$, $\beta = 0.1$, $n = 1$, $\omega = 0.1$, $\sigma = 0.1$, $\varphi = 0.01$, and $S = 0.1$.

It can be observed in Figs 14–18 that the solutal boundary layer thickness diminishes with increasing values of the thermophoresis parameter, Lewis number, reaction rate parameter, reaction constant and Biot number. The Lewis number degrades the molecular diffusion rate while the chemical reaction rate parameter dilutes the concentration of the Al_2O_3 oil-based nanofluid. Similarly, the chemical reaction rate parameter accelerates the rate of mass transfer to increase the concentration gradient which deteriorates the solutal boundary layer thickness.

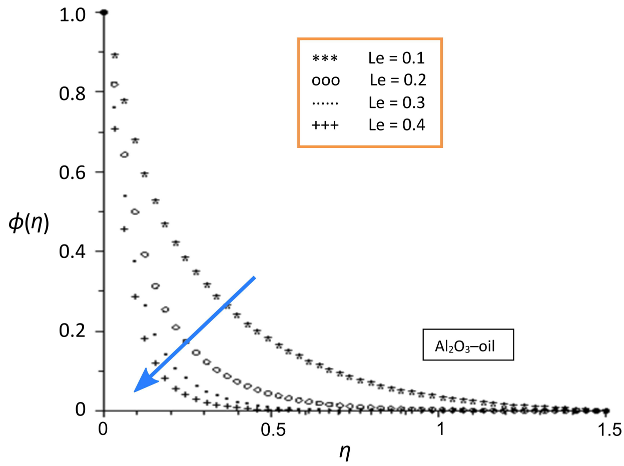

FIG. 15. Concentration profile for varying values of the Lewis number for $\alpha = 1$, $S = 0.1$, $K^* = 0.5$, $\mathrm{Bi} = 0.1$, $\lambda = 1$, $n = 1$, $\sigma = 0.1$, $E = 0.1$, $\beta = 0.1$, $\mathrm{Pr} = 100$, $\omega = 0.1$, $\mathit{\Gamma} = 0.1$, $\mathrm{Ec} = 0.01$, and $\varphi = 0.01$.

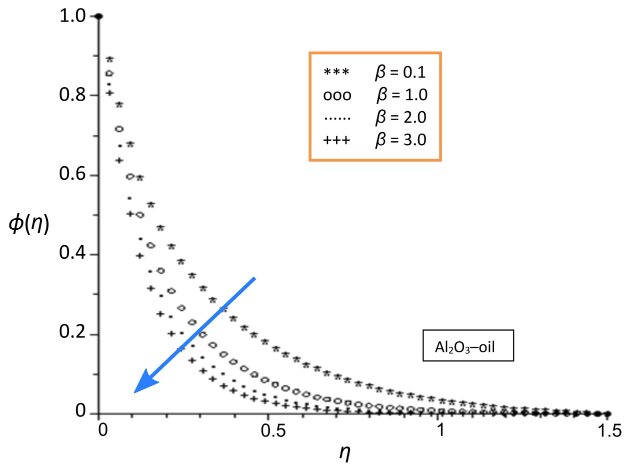

FIG. 16. Concentration profile for varying values of chemical reaction rate parameter for $\mathrm{Pr} = 100$, $\alpha = 1$, $K^* = 0.1$, $\mathrm{Ec} = 0.01$, $\lambda = 1$, $\mathrm{Le} = 0.1$, $\sigma = 0.1$, $E = 0.1$, $\mathrm{Bi} = 0.1$, $n = 1$, $\omega = 0.1$, $\mathit{\Gamma} = 0.1$, $\varphi = 0.01$, and $S = 0.1$.

6. CONCLUSIONS

The influence of thermophoretic transport of Al_2O_3 nanoparticles on heat and mass transfer of viscoelastic flow of oil-based nanofluid past a porous exponentially stretching surface with activation energy has been discussed. The study revealed that:

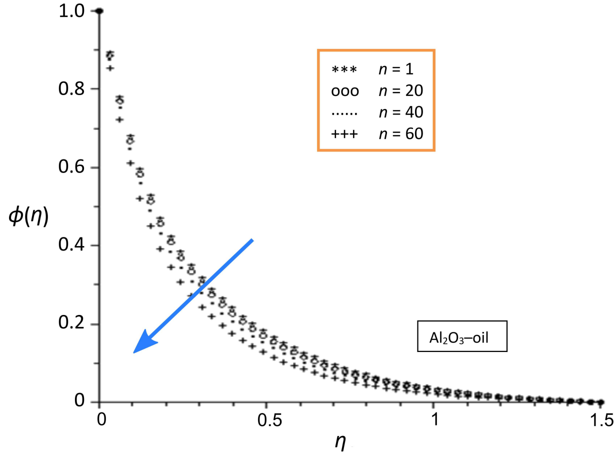

FIG. 17. Concentration profile for varying values of fitted rate constant for $\alpha = 1$, $S = 0.1$, $K^* = 0.5$, $\mathrm{Bi} = 0.1$, $\lambda = 1$, $\mathrm{Le} = 0.1$, $\sigma = 0.1$, $E = 0.1$, $\beta = 0.1$, $\mathrm{Pr} = 100$, $\omega = 0.1$, $\Gamma = 0.1$, $\mathrm{Ec} = 0.01$, and $\varphi = 0.01$.

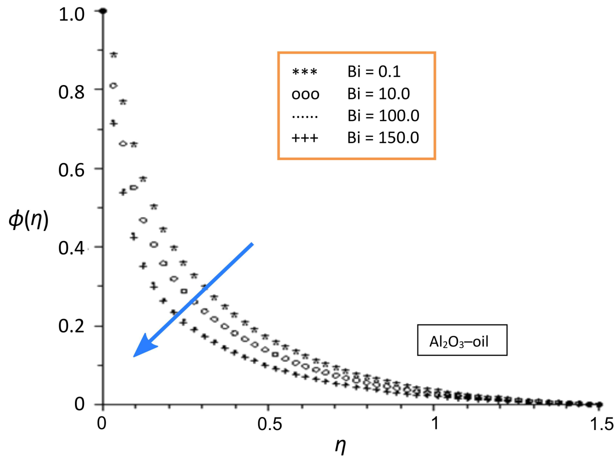

FIG. 18. Concentration profile for varying values of Biot number for $\mathrm{Pr} = 100$, $\alpha = 1$, $K^* = 0.1$, $\mathrm{Ec} = 0.01$, $\lambda = 1$, $\mathrm{Le} = 0.1$, $\sigma = 0.1$, $E = 0.1$, $\beta = 0.1$, $n = 1$, $\omega = 0.1$, $\Gamma = 0.1$, $\varphi = 0.01$, and $S = 0.1$.

1) The viscoelasticity and permeability of the flow can be used to control the nanofluid kinematics.
2) The internal heat generation and the thermal conductivity are important parameters to control the thermal dynamics of the flow.
3) The thermophoresis parameter and the reaction rate parameter are important when it is desired to reduce the chemical reaction during the flow of the Al_2O_3 nanoparticles in the oil-based nanofluid.

References

1. Baaske P., Wienken C.J., Reineck P., Duhr S., Braun D., *Optical thermophoresis for quantifying the buffer dependence of aptamer binding*, Angewandte Chemie International Edition, **49**(12): 2238–2241, 2010.

2. Chao Z., Jinxin F., Alparslan O., Xuanhong C., *Measuring the Soret coefficient of nanoparticles in a dilute suspension*, Journal of Nanoparticle Research, **16**(10): 1–11, 2014.

3. Loganathan P., Arasu P.P., *Thermophoresis effects on non-Darcy MHD mixed convective heat and mass transfer past a porous wedge in the presence of suction/injection*, Theoretical Applied Mechanics, **37**(3): 203–227, 2010.

4. Thamdrup L.H., Larsen N.B., Kristensen A., *Light-induced local heating for thermophoretic manipulation of DNA in polymer micro- and nanochannels*, Nano Letters, **10**(3): 826–832, 2010.

5. Kishan N., Jagadha S., *Thermophoresis and chemical reaction effects on MHD Darcy-Forchheimer mixed convection in a fluid saturated porous media*, International Journal of Engineering Trends and Technology, **10**(5): 235–243, 2014.

6. Ghadam A.G.J., Moradi A., *Effects of Brownian motion and thermophoresis on MHD mixed convection stagnation-point flow of a nanofluid toward a stretching vertical sheet in porous medium*, Journal of Particle Science and Technology, **1**: 225–240, 2015.

7. Rashad A.M., Mallikarjuna B., Chamkha A.J., Raju S.H., *Thermophoresis effect on heat and mass transfer from a rotating cone in a porous medium with thermal radiation*, Afrika Matematika, **27**(7–8): 1409–1424, 2016.

8. Falana A., Ojewale O.A., Adeboje T.B., *Effect of Brownian motion and thermophoresis on a nonlinearly stretching permeable sheet in a nanofluid*, Advances in Nanoparticles, **5**: 123–134, 2016.

9. Raju K.V., Reddy P.B.A., Suneetha S., *Thermophoresis effect on a radiating inclined permeable moving plate in the presence of chemical reaction and heat absorption*, International Journal of Dynamics of Fluids, **13**(1): 89–112, 2017.

10. Shafique Z., Mustafa M., Mushtaq A., *Boundary layer flow of Maxwell fluid in rotating frame with binary chemical reaction and activation energy*, Results in Physics, **6**: 627–633, 2016.

11. Mustafa M., Mushtaq A., Hayat T., Alsaedi A., *Numerical study of MHD viscoelastic fluid flow with binary chemical reaction and Arrhenius activation energy*, International Journal of Chemical Reactor Engineering, **15**(1): 1–9, 2016.

12. Monica M., Sucharitha J., Kishore C.H., *Effects of exothermic chemical reaction with Arrhenius activation energy, non-uniform heat source/sink on MHD stagnation point flow of a Casson fluid over a nonlinear stretching sheet with variable fluid properties and slip conditions*, Journal of the Nigerian Mathematical Society, **36**: 163–190, 2017.

13. Anuradha S., Sasikala K., *MHD mixed convection stagnation point flow with binary chemical reaction and activation energy*, International Journal of Engineering and Techniques, **3**(6): 320–324, 2017.

14. Kiran Kumar R.V.M.S.S., Kumar G.V., Raju C.S.K., Shehzad S.A., Varma S.V.K., *Analysis of Arrhenius activation energy in magnetohydrodynamic Carreau*

fluid flow through improved theory of heat diffusion and binary chemical reaction, Journal of Physics Communications, **2**(3): 1–14, 2018.

15. Choi S.U.S., Eastman J.A., *Enhancing thermal conductivity of fluids with nanoparticles*, Developments Applications of Non-Newtonian Flows, ASME, New York, FED-Vol. 231/MD-Vol. 66, pp. 99–105, 1995.
16. Jakati S.V., Raju B.T., Nargund A.L., Sathyanarayana S.B., *The Effect of Brownian motion and thermophoresis on nanofluids stretching for Jaffrey fluid model*, International Journal of Latest Transactions in Engineering and Science, **3**(3): 1–9, 2018.
17. Anuradha S., Sasikala K., *MHD free convective flow of a nanofluid over a permeable shrinking sheet with binary chemical reaction and activation energy*, International Journal of Engineering Science Invention, **7**(1): 22–30, 2018.
18. Zeeshan A., Shehzad N., Ellahi R., *Analysis of activation energy in Couette-Poiseuille flow of nanofluid in the presence of chemical reaction and convective boundary conditions*, Results in Physics, **8**: 502–512, 2018.
19. Brinkman H.C., *Viscosity of concentrated suspensions and solutions*, The Journal of Chemical Physics, **20**: 571–581, 1952.
20. Bidin B., Nazar R., *Numerical solution of the boundary layer flow over an exponentially stretching sheet with thermal radiation*, European Journal of Scientific Research, **33**(4): 710–717, 2009.

Received August 15, 2018; accepted version February 27, 2019.